

CONVERGENCE OF MULTI-POINT FLUX APPROXIMATIONS ON GENERAL GRIDS AND MEDIA

RUNHILD A. KLAUSEN AND ANNETTE F. STEPHANSEN

Abstract. The analysis of the Multi Point Flux Approximation (MPFA) method has so far relied on the possibility of seeing it as a mixed finite element method for which the convergence is then established. This type of analysis has been successfully applied to triangles and quadrilaterals, also in the case of rough meshes. The MPFA method has however much in common with another well known conservative method: the mimetic finite difference method. We propose to formulate the MPFA O-method in a mimetic finite difference framework, in order to extend the proof of convergence to polyhedral meshes. The formulation is useful to see the close relationship between the two different methods and to see how the differences lead to different strenghts. We pay special attention to the assumption needed for proving convergence by examining various cases in the section dedicated to numerical tests.

Key Words. Polygonal and polyhedral mesh, convergence, multi-point flux approximation, MPFA O-method, mimetic finite difference.

1. Introduction

When solving problems on a geological structure, one of the challenges that confronts numerical methods is grid deformation. In reservoir simulation a lot of work goes into making geological models. The models incorporate results both from direct measurements in the reservoir and statistical information from outcrops on land. The end result is a model that has a vertical resolution from around 20 cm to about a meter. Due to the size of the domain and the need to limit the size of the calculations, the vertical resolution of a typical simulation block lies between 5 and 20 meters. While the usual approach is to smooth out geological features, there is also a call for using more flexible grids. This includes grids that are heavily distorted as well as going beyond the standard quadrilaterals or hexahedra. The problem of grid deformation comes in addition to challenges such as anisotropies and discontinuities in the geological media due to layering and fractures.

One family of methods proposed for calculating the Darcy flow in reservoir simulation is the multi-point flux approximation (MPFA) methods. These have mostly been applied on quadrilaterals/hexahedra, though triangles and polygons have also been tested, see e.g. [2, 3, 18, 11]. While the MPFA methods have numerically been shown to converge, eg. [13, 24, 25], it has proved more difficult to prove the convergence analytically. Considering the theoretical convergence analysis, initial attempts sought how to reconstruct an interior vector field compatible with the fluxes which would recast the MPFA method as a mixed finite element method. An example of how the standard MPFA O-method is recast as a mixed finite element

Received by the editors February 10, 2011, and in revised form, June 29, 2011.
2000 *Mathematics Subject Classification.* 35R35, 49J40, 60G40.

(MFE) method on triangulations can be found in [28, 18]. In [21, 29], examining quadrilaterals, an MPFA O-method which is derived from a mapping onto an orthogonal reference cell is analyzed. In a successive paper convergence is proved for the MPFA O-method on rough grids [22]. A new proof of convergence of the MPFA O-method on general grids has been presented by Agelas and Masson [7]. Here they show weak convergence of the gradient, but do not provide rate of convergence of the fluxes. Their proof is however valid on heterogeneous permeability fields and is not based on similarities with the MFE methods. In the recent papers by Bause, Hoffmann and Knabner, cf. [8], Matringe, Juanes and Tchelep, cf. [30] and Ingram, Wheeler and Yotov, cf. [16], convergence of MPFA method is shown on the special cases of triangulations, parallelepipeds and hexahedra respectively. These papers are based on the relationship between the MFE method and the quadrature from [22]. In Klausen and Stephansen [20] the MPFA O-method in 2D is written as a mimetic finite difference (MFD) method by using the same quadrature from [22] but which then allows for general meshes. The paper includes a sketch of a convergence proof. The present paper is an extension of the ideas from [20], and the proof closely follows that of the articles [9, 23] on mimetic finite difference methods.

The aforementioned MFD method is known for its flexibility, as it can be defined on polygons or polyhedra and can be applied with grids presenting hanging nodes, see e.g. [1, 9]. In addition it converges even when the grid is heavily distorted or the anisotropy ratio of the permeability is high. What is less known is the close tie between the MFD method and the MPFA methods. Both classify for instance as raw field methods, in contrast to full field methods like the MFEM, cf. [17]. However, the differences are also important as they lead to different properties of the methods. In particular we note that the symmetry of the MFD method is what makes it so robust, as the mass matrix is tailored by the user to always be positive definite. On the other hand, this symmetry implies that the fluxes are globally coupled. Explicit local fluxes are useful in two-phase flow simulations, as the discretization for one-phase flow fluxes is easily updated by multiplying with the scalar mobility. It is in fact the discretization for explicit local fluxes that is the strength of the MPFA O-method. The price to pay is the loss of symmetry of the latter method, which impairs the convergence properties. We note that the standard implementation of the two methods is fundamentally different. While the MFD method involves solving a saddle point problem, the MPFA O-method is a finite volume scheme. We will however use the similarities between the two methods to prove convergence of the MPFA O-method.

We will show that a family of MPFA O-methods may be implemented as a MFD method. In fact, we will show that the MPFA O-method coincides with the local flux MFD method [23] when the latter uses a version of non-symmetric quadrature proposed in [22]. As the local flux MFD method is shown to converge on general polygons or polyhedra, this result applies to the MPFA O-method as well. We show how the analysis may be extended to include discontinuities in the permeability field as well.

The non-symmetry of the MPFA O-method poses an important limitation on the convergence proof in terms of what anisotropy ratios and grid deformations are permitted. However, the non symmetry of the method is what permits us to calculate local fluxes explicitly while still maintaining a limited stencil and obtaining convergence on rough grids. It should not therefore be seen as a fault of the method. It does mean though that extension to general polygons or polyhedra is not as straight forward as expected, as even too large grid deformations on quadrilaterals pose an

important problem. We examine aspects and limitations of the non-symmetric quadrature in the numerical section. We are also interested in whether or not the assumption is sharp. We therefore examine the convergence of the pressure and of the flux using a comparable norm on a grid where the assumption necessary for the convergence proof is no longer satisfied. To complete the paper we have added two numerical tests illustrating the convergence results. For further tests regarding the convergence properties of the MPFA O-method the previously cited papers may be consulted.

The paper is organized as follows: Section 2 presents the model problem and setting. Section 3 provides the convergence proof, while Section 4 presents numerical tests which provide the basis for discussing the validity of the convergence proof.

2. Model problem and setting

2.1. Continuous problem. For simplicity of exposition we will limit our discussion to homogeneous Dirichlet boundary conditions. Let Ω be a domain in \mathbb{R}^d , $d \in \{2, 3\}$, with polygonal boundary $\partial\Omega$. We consider the following elliptic equation:

$$(1) \quad \begin{cases} -\nabla \cdot (K \nabla p) = f & \text{in } \Omega, \\ p = 0 & \text{on } \partial\Omega. \end{cases}$$

Viewing (1) as the prototype for the pressure equation in porous medium flow, we can identify p as the pressure, K as the permeability tensor and f as a source term.

The mixed formulation of (1) is obtained by introducing the unknown Darcy velocity $\mathbf{u} = -K \nabla p$ as a new variable. We seek $(\mathbf{u}, p) \in H(\text{div}, \Omega) \times L^2(\Omega)$ such that

$$(2) \quad \begin{cases} (K^{-1} \mathbf{u}, \mathbf{v})_{0, \Omega} - (p, \nabla \cdot \mathbf{v})_{0, \Omega} = 0, & \forall \mathbf{v} \in H(\text{div}, \Omega), \\ (\nabla \cdot \mathbf{u}, q)_{0, \Omega} = (f, q)_{0, \Omega} & \forall q \in L^2(\Omega), \end{cases}$$

where $f \in L^2(\Omega)$ and K is a symmetric, positive definite field whose eigenvalues are bounded. The smallest eigenvalue is bounded away from zero. The subscript $0, \Omega$ denotes the L^2 -scalar product on Ω . Similarly, the subscript $0, R$ indicates the L^2 -scalar product and its associated norm on a subset $R \subset \Omega$. For $s \geq 1$, a norm (semi-norm) with the subscript s, R designates the usual norm (semi-norm) in $H^s(R)$.

2.2. Discontinuous media and regularity. The MPFA method was originally designed to handle rough grids and eliminate the grid effect that is seen with use of e.g. the two-point flux approximation (TPFA) method. In rough grids the grid lines follow natural variations in the geological media. The resulting coefficients used to describe these natural variations in the media will therefore also be discontinuous. The most dominant cause of discontinuities is probably the layering in the media, but also fractures may result in essential discontinuities. In addition to this, the geologists model the media quite neatly, with permeability varying from cell to cell in the geological model, cf. for instance Figure 1. These geological models are still too fine for simulations, but as computer and models develop, simulations on such models is a final goal.

The permeability K is modeled by a symmetric positive definite tensor. In the same way as roughness of the grid is fundamental, the main direction of the permeability will vary and result in a full tensor. It is an important feature of reservoir simulation that K is allowed to be discontinuous, and the MPFA method and the MFD method have been applied to such cases. However, for the convergence

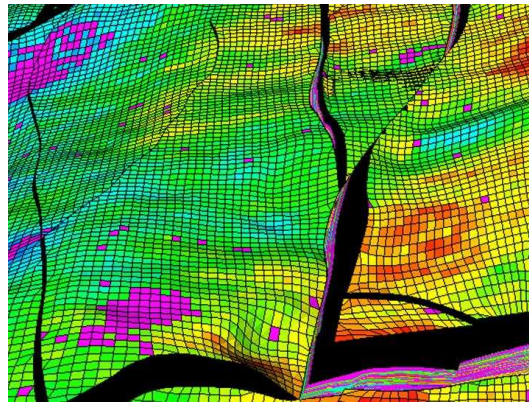


FIGURE 1. *A geological grid, with layers, fractures and highly varying permeability*

analysis both the solution and the coefficients are usually supposed to be very regular. In particular, the Darcy velocity and the pressure are supposed to satisfy

$$(3) \quad \mathbf{u} \in (H^1(\Omega))^2 \quad \text{and} \quad p \in H^2(\Omega).$$

This regularity is for example ensured if the domain Ω is convex, $f \in L^2$ and the permeability is continuous. In special cases discontinuous coefficients still give some smoothness of the solution, and for such cases relaxed smoothness conditions on the permeability are allowed. The most interesting extension from our point of view is the case of layered media, where eq. (3) extend for media with smooth boundaries, which locally may be mapped to a straight lines. While the gradient of the solution is discontinuous, the solution is still in H^2 .

In general, piecewise regularity will not imply global regularity. In cases where singularities arise the global regularity will depend on the permeability and its distribution. For an in-depth discussion one may consult [26]. For cases with discontinuous permeability around corners (as will arise when grid blocks with different permeabilities meet in a vertex) we have

$$(4) \quad \mathbf{u} \in (H^\xi(\Omega))^d \quad \text{and} \quad p \in H^{1+\xi}(\Omega),$$

where the interpolated Hilbert space $H^{1+\xi+\epsilon}$ is defined for all $\epsilon > 0$, and for $0 < \xi < 1$, see [27, Chapter 8].

Lately convergence has been examined in cases where less regularity of the solution is required. For the MPFA methods we mention the work by Klausen, Radu and Eigestad [18], which regards the Richards' equation on triangular grids, and the work by Agelas and Masson [7] on the elliptic equation on general grids. The techniques involved in the latter paper are very different from those used in the analysis of the present paper and are based on [14].

2.3. Discrete setting and interpolation. Regarding notation, a tilde will indicate an integrated quantity, such as fluxes or a normal integrated over the corresponding (partial) face. The subscript h indicates a member of the discrete space, while bolds will indicate a vector.

Let $\{\mathcal{P}_h\}_{h>0}$ be a shape-regular family of affine polyhedral meshes of the domain Ω . For definitions regarding shape-regularity we refer to [9]. A generic element in \mathcal{P}_h is denoted by E , h_E denotes the diameter of E and \mathbf{n}^E its outward unit normal.

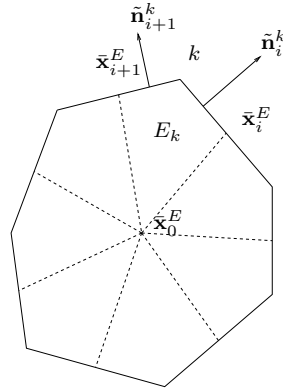


FIGURE 2. *Nomenclature in 2D*

Set $h = \max_{E \in \mathcal{P}_h} h_E$. The nodes of the element form the set \mathcal{N}^E , while the nodes of the face F_i form the set \mathcal{N}_i^E . In 3D we require that each polyhedron be such that a maximum of 3 faces meet in a vertex (node). The reason for this limitation will be explained next, and is due to the possibility to split each element E into subelements E_k which are used for the definition of the MPFA O-method.

We denote the barycenter of the element E with \bar{x}_0^E , the barycenter of the faces with \bar{x}_i^E and the barycenter of the edges with \bar{x}_e^E . The partial faces of the subelements E_k which are also partitions of F_i are denoted by F_{ik} . To each of the faces F_{ik} we associate the normal $\tilde{\mathbf{n}}_{ik}$ which is \mathbf{n}_i^E (the normal of F_i) integrated over the partial face F_{ik} . The notation is illustrated in Figure 2. Note that $\tilde{\mathbf{n}}_{ik}$ has the dimension of a length in 2D. In the definition of the MPFA O-method we also use the edge vectors $(\bar{x}_i^E - \bar{x}_0^E, \bar{x}_{i+1}^E - \bar{x}_0^E)$, cf. eq (15). As will be seen in the following Remark, these vectors create edges of the subelements E_k that are quadrilaterals in 2D and deformed cubes with straight edges in 3D. With a deformed cube we intend a cell similar to a hexahedron in shape, described by eight vertices and twelve straight edges. We are not interested in the general faces here, which might be bilinear and not uniquely defined.

Remark 1. *In 2D all convex polygons can be split into k quadrilaterals, where k is the number of vertices. Under the condition that 3 faces meet in each vertex, all convex polyhedra can be split into k deformed cubes with straight edges.*

In 2D we split the polygon by connecting the barycenter of each face with the barycenter of the element itself. A quadrilateral E_k is then defined by connecting the following four points with four non-intersecting straight lines: the barycenter of the element, the node k and the barycenters of the two faces that meet in the node k . The points are defined independently of the node and the sum of the quadrilaterals therefore covers the polygon. An illustration is found in Figure 2.

For the 3D case we need 8 points to be able to define a deformed cube. We will use the barycenters of the faces as well as the barycenters of the edges. The subelement E_k is constructed from the barycenter of the cell (1 point), one vertex k (1 point), the barycenters of the 3 faces that have the vertex k in common (3 points), and the barycenters of the 3 edges that meet in the vertex k (3 points). This gives us 8 points associated with each vertex or node k . By connecting these points with 12 non-intersecting straight lines we have formed the edges of the deformed cube. The faces that are in common with the faces of the polyhedron itself will be plane, while the faces interior to the element are possibly bilinear. While not

uniquely defined, it is possible to define the bilinear faces such that the volume covered by these subelements is the same as the volume of the polyhedron, and the intersecting volume of the sub-elements is zero.

We note that the exact definition of the internal faces of the deformed cubes are not needed in the definition of the MPFA method; only the edges of the cube and the faces coinciding with the faces of the original polyhedron are used, all of which are uniquely defined. The MPFA-method is designed for use on grids like the corner-point grid [31], where the majority of cells will be deformed cubes. However, this type of grid is much more general, allowing for instance collapsed cells where some of the nodes coincide or grid cells with non-matching faces. We will not consider such general grids here.

We consider the space X_h of discrete pressures that are constant on each element E , that is,

$$X_h = \{q_h \in L^2(\Omega); \forall E \in \mathcal{P}_h, q_h|_E \in \mathbb{P}_0\}.$$

where \mathbb{P}_0 indicates polynomials of degree 0. Our velocity space V_h consists of discrete velocity vectors defined only on the partial faces F_{ik} of the element and are aligned with the average normal of the partial face. To each face F_i of the element E we thus associate $m_i = \#\mathcal{N}_i^E$ unknowns, where $\#\mathcal{N}_i^E$ is the number of vertexes of the face i . These unknowns are the (scalar) partial fluxes $\tilde{v}_{ik}^E, k \in \mathcal{N}_i^E$. The discrete velocity field is thus defined by its components that are piecewise constant on a face and equal to

$$(5) \quad \mathbf{v}_{ik}^E = \frac{1}{|F_{ik}|} \tilde{v}_{ik}^E \hat{\mathbf{n}}_{ik}^E$$

where

$$\hat{\mathbf{n}}_{ik}^E = \frac{\tilde{\mathbf{n}}_{ik}^E}{|\tilde{\mathbf{n}}_{ik}^E|} = \frac{\tilde{\mathbf{n}}_{ik}^E}{|F_{ik}|}$$

is the unit average normal vector on the partial face F_{ik} . In addition, conservation of flux is imposed directly on the partial fluxes. This imposes continuity of the normal component of the velocity field. As fluxes aligned with the outward normal are defined as positive, on a partial side shared by two elements the sum of the corresponding partial fluxes must be equal to zero. We also define the flux \tilde{v}_i over the face F_i equal to the sum of the corresponding partial fluxes, i.e.

$$(6) \quad \tilde{v}_i^E = \sum_{k \in \mathcal{N}_i^E} \tilde{v}_{ik}^E.$$

The superscript E will henceforward be omitted if there is no ambiguity in order to facilitate reading. The partial side fluxes are regrouped into the vector $\tilde{\mathbf{v}}$, while the restriction of $\tilde{\mathbf{v}}$ to the partial fluxes on the faces F_{ik} that share a vertex k is indicated by $\tilde{\mathbf{v}}_k$.

To comply with the mimetic finite difference setting, we define the discrete divergence of $\mathbf{v}_h \in V_h$ as an operator $\nabla_h : V_h \mapsto X_h$ such that on each $E \in \mathcal{P}_h$

$$(7) \quad \nabla_h \cdot \mathbf{v}_h|_E \equiv \frac{1}{|E|} \sum_{F_i \in \partial E} \tilde{v}_i^E = \frac{1}{|E|} \sum_{F_i \in \partial E} \sum_{k \in \mathcal{N}_i^E} \tilde{v}_{ik}^E.$$

Finally we define the interpolation operator \mathcal{I} of any vector-valued function $\mathbf{v} \in H(\text{div}, \Omega)$ so that $\mathbf{v}^{\mathcal{I}} \in V_h$ and

$$(8) \quad (\mathbf{v}^{\mathcal{I}})_{ik} = \frac{1}{|F_{ik}|} (\mathbf{v} \cdot \mathbf{n}_i^E, 1)_{0, F_{ik}} \hat{\mathbf{n}}_{ik} \quad \forall E \in \mathcal{P}_h, \forall F_{ik} \in F_i.$$

The interpolation thus gives a piece-wise constant velocity vector directed in the average normal direction of the sub-face F_{ik} , given by the average flux divided by the area. An important property of this interpolation is that the flux over each sub-face F_{ik} (and thus over each face $F_i \in \partial E$) is preserved, i.e.

$$\begin{aligned} ((\mathbf{v}^{\mathcal{I}})_{ik} \cdot \mathbf{n}_i^E, 1)_{0, F_{ik}} &= (\mathbf{v}^{\mathcal{I}})_{ik} \cdot \tilde{\mathbf{n}}_{ik} = \frac{1}{|F_{ik}|} (\mathbf{v} \cdot \mathbf{n}_i^E, 1)_{0, F_{ik}} \hat{\mathbf{n}}_{ik} \cdot \tilde{\mathbf{n}}_{ik} \\ (9) \qquad \qquad \qquad &= (\mathbf{v} \cdot \mathbf{n}_i^E, 1)_{0, F_{ik}} \end{aligned}$$

It immediately follows that the discrete divergence (defined in (7)) of the interpolation function is equal to the L^2 projection on E of the divergence of the continuous function. That is, using (9),

$$\begin{aligned} \nabla_h \cdot \mathbf{v}^{\mathcal{I}}|_E &= \frac{1}{|E|} \sum_{F_i \in \partial E} \sum_{k \in \mathcal{N}_i^E} ((\mathbf{v}^{\mathcal{I}})_{ik} \cdot \mathbf{n}_i^E, 1)_{0, F_{ik}} = \frac{1}{|E|} \sum_{F_i \in \partial E} (\mathbf{v} \cdot \mathbf{n}_i^E, 1)_{F_i} \\ (10) \qquad \qquad &= \frac{1}{|E|} (\nabla \cdot \mathbf{v}, 1)_{0, E}. \end{aligned}$$

In particular, by setting $\mathbf{u} = -K \nabla p$ we see that

$$(11) \qquad \nabla_h \cdot \mathbf{u}_h^{\mathcal{I}} = \frac{1}{|E|} (\nabla \cdot (-K \nabla p), 1)_{0, E} = \frac{1}{|E|} (f, 1)_{0, E},$$

a result which will be used in the convergence proof.

Finally, we will make the following hypothesis on the permeability tensor: There exists a piecewise continuous field K_0^E , symmetric and positive definite with bounded eigenvalues, such that

$$(12) \qquad \|K - K_0^E\|_{L^\infty(E)} \lesssim h_E \quad \forall E \in \mathcal{P}_h.$$

This assumption limits the variation of permeability within each element, but allows for discontinuities from one element to another. For proving convergence of the pressure further regularity of the permeability field will have to be assumed.

2.4. Reformulation of MPFA. The MFD method defines a quadrature for each element with a quadrature matrix that is symmetric, positive definite and full. Only one unknown is specified for each face. The MPFA method is designed to give explicit local fluxes, a property that requires that the number of unknowns to be expanded. However, the resulting quadrature matrix Λ is sparse, with non-zero elements only if the partial fluxes share a vertex. The quadrature over the element E can therefore be decomposed into the sum of local quadratures with matrices that are of size $d \times d$, i.e. for $\mathbf{u}_h, \mathbf{v}_h \in V_h$:

$$(13) \qquad [\mathbf{u}_h, \mathbf{v}_h]_E = \tilde{\mathbf{v}}_h^t \Lambda^E \tilde{\mathbf{u}}_h = \sum_k \tilde{\mathbf{v}}_{h,k}^t \Lambda_k \tilde{\mathbf{u}}_{h,k}$$

where the quadrature matrix Λ^E depends on the permeability and the mesh geometry. We set K_0^E equal to the constant permeability tensor on E as seen in (12). The MPFA quadrature matrix Λ_k for the O-method is then defined for each partial quadrilateral or deformed cube E_k , cf. Remark 1, as

$$(14) \qquad \Lambda_k = R_k (K_0^E)^{-1} Q_k^{-t}.$$

Indicating by $i1, i2, i3$ the three partial faces that share the vertex k of element E (in 2D any reference to $i3$ is simply eliminated), the two matrices R_k and Q_k are defined, as

$$(15) \qquad R_k = (\bar{\mathbf{x}}_{i1} - \bar{\mathbf{x}}_0, \bar{\mathbf{x}}_{i2} - \bar{\mathbf{x}}_0, \bar{\mathbf{x}}_{i3} - \bar{\mathbf{x}}_0)^t \quad \text{and} \quad Q_k = (\tilde{\mathbf{n}}_{i1}, \tilde{\mathbf{n}}_{i2}, \tilde{\mathbf{n}}_{i3}).$$

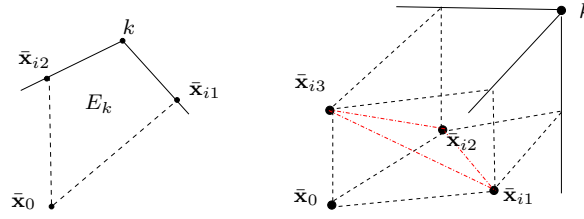


FIGURE 3. Subelement E_k in 2 and 3 dimension

We define the scalar product on X_h as

$$(16) \quad (p_h, q_h)_{X_h} = \sum_{E \in \mathcal{P}_h} (p_h, q_h)_{0,E} \quad \forall p_h, q_h \in X_h$$

The discrete version of (2) using the MPFA quadrature is then: find $(\mathbf{u}_h, p_h) \in (V_h, X_h)$ such that

$$(17) \quad \begin{cases} \sum_{E \in \mathcal{P}_h} [\mathbf{u}_h, \mathbf{v}_h]_E - (p_h, \nabla_h \cdot \mathbf{v}_h)_{X_h} = 0 & \forall \mathbf{v}_h \in V_h, \\ (\nabla_h \cdot \mathbf{u}_h, q_h)_{X_h} = (f, q_h)_{0,\Omega} & \forall q_h \in X_h. \end{cases}$$

The first line of (17) represents the half edge fluxes as functions of pressure differences. All subelements with a common cell vertex create a dual cell, on which we from (17) have a locally invertible set of equations. When this inversion is carried out for each dual cell, the resulting equations yield the traditional explicit MPFA flux formulation, i.e the next Lemma.

Lemma 2. *The set of equations in (17) coincides with the MPFA O-method formulation as presented for instance in [2, 3] after a local inversion of the equations on dual cells.*

Proof. We start by the basic assumption of MPFA which is linear pressure variation over the $\{\bar{\mathbf{x}}_0, \bar{\mathbf{x}}_{i1}, \bar{\mathbf{x}}_{i2}, \bar{\mathbf{x}}_{i3}\}$ -tetrahedra, cf. Figure 3. Define the local vectors $\bar{\mathbf{p}}_k = (\bar{p}_{i1}, \bar{p}_{i2}, \bar{p}_{i3})^t$ and $\bar{\mathbf{p}}_0 = \bar{p}_0(1, 1, 1)^t$, where \bar{p}_{ij} is an approximation of the pressure at $\bar{\mathbf{x}}_{ij}$, $j \in \{1, 2, 3\}$. The constant gradient over the actual tetrahedra can then be found as

$$\nabla p = R_k^{-1}(\bar{\mathbf{p}}_k - \bar{\mathbf{p}}_0),$$

since the matrix R_k contains the lengths between the pressure points. More details can for instance be found in [3]. Using the constant permeability tensor K_0 defined by (12), the Darcy flux through a face F_{ij} is $u_{ij} = -K_0 \nabla p \cdot \tilde{\mathbf{n}}_{ij}$. The Darcy fluxes through the partial faces F_{ik} of E_k are then expressed as

$$(18) \quad \tilde{\mathbf{u}}_k = -Q_k^t K_0 \nabla p = \Lambda_k^{-1}(\bar{\mathbf{p}}_0 - \bar{\mathbf{p}}_k),$$

with $\tilde{\mathbf{u}}_k = (\tilde{u}_{i1}, \tilde{u}_{i2}, \tilde{u}_{i3})^t$. In early MPFA papers like eg. [2, 3, 11], a local explicit multi point flux expression is defined by eliminating all edge pressures \bar{p}_j on dual gridcells consisting of all subelements with a common vertex. If we instead invert Λ_k^{-1} of (18) we obtain

$$\Lambda_k \tilde{\mathbf{u}}_k = (\bar{\mathbf{p}}_0 - \bar{\mathbf{p}}_k)$$

which we multiply on both sides with arbitrary half-side fluxes $\tilde{\mathbf{v}}_k$ to obtain

$$(19) \quad \tilde{\mathbf{v}}_k^t \Lambda_k \tilde{\mathbf{u}}_k = \tilde{\mathbf{v}}_k^t (\bar{\mathbf{p}}_0 - \bar{\mathbf{p}}_k).$$

Noting that on neighboring elements the pressure \bar{p}_{ij} is the same while the flux \tilde{v}_{ik} changes sign, we have that

$$-\sum_{E,k \in \mathcal{N}^E} \tilde{\mathbf{v}}_k^t \bar{\mathbf{p}}_k = 0.$$

From the definition of discrete divergence (7) we have

$$\sum_{E,k \in \mathcal{N}^E} \tilde{\mathbf{v}}_k^t \bar{\mathbf{p}}_0 = \sum_E \bar{p}_0 \sum_k \tilde{v}_{ik} = \sum_E |E| \bar{p}_0 \nabla_h \cdot \mathbf{v}_h|_E = (p_h, \nabla_h \cdot \mathbf{v}_h)_{X_h},$$

where the latter equality comes from the definition of the scalar product on X_h (16). We therefore see that summing equation (19) over all the elements we obtain the first line in (17). The second line is quite simply the finite volume formulation of MPFA, stating that the sum of the fluxes out of an element equals to the volume average of the source over the element. This is easily seen by setting q_h equal to one on the element in question and zero elsewhere.

The MPFA formulation found from (18) is therefore equivalent to the MPFA formulation in (17) by inversion of Λ . \square

A more detailed 2D calculation of the passage between the two different formulations of the MPFA O-method can be found in the Appendix of [22]. The two MPFA formulations can be classified as K and K^{-1} methods, where (17) is a K^{-1} method, cf. [19]. The K method avoids the difficulty of solving a saddle point problem and gives explicit local fluxes. The quadrature formulation is however useful to analyze the convergence of the method, as we shall see. The MPFA O-method is actually an entire family of methods, where the choice of $\bar{\mathbf{x}}_{ij}$ on the faces can vary. The results above extends to the whole family, but with different vectors creating the R_k matrix.

We note that the (symmetric) elliptic problem is now discretized using an MPFA inner product (13) that is now non-symmetric. In fact, the coefficients of Λ_k become

$$\lambda_{rs} = \frac{1}{\det(R_k)} (\bar{\mathbf{x}}_{ir} - \bar{\mathbf{x}}_0) K^{-1} \tilde{\mathbf{n}}_{is}.$$

Only if $R_k = Q_k^{-1}$ do we have symmetry, which is the case of grids that are constructed with parallelograms for instance. We note that if all the off diagonal elements of Λ are zero the mesh is classified as a K -orthogonal mesh.

This general lack of symmetry might seem a weakness, and indeed the standard MFD is always defined with a symmetric inner product. However, when splitting the flux to gain a local flux, the non-symmetry is the price to pay to have convergence on general grids. The article [5] contains a numerical study of a symmetric versus a non-symmetric MPFA O-method which highlights this point. Insisting on this type of symmetric (and sparse) inner product will mean that convergence is only obtained if the subelements of the refined grid approach parallelograms. Constructing a family of such grids from of hexahedra mesh is easy, but this will not be the case for more general polygonal meshes.

2.5. Energy norm and assumption. We note that while the term $[\mathbf{u}_h, \mathbf{v}_h]_E$ is a scalar product when the mimetic finite difference method is used, this is in general not the case for the MPFA method, as Λ_k can be non-symmetric. However, the matrix Λ^E can be decomposed into its symmetric and skew-symmetric parts

$$(20) \quad \Lambda^E = \frac{1}{2}(\Lambda + \Lambda^t) + \frac{1}{2}(\Lambda - \Lambda^t) = \Lambda_S + \Lambda_A$$

and similarly $\Lambda_k = (\Lambda_S)_k + (\Lambda_A)_k$. We define the following scalar product on V_h :

$$(\mathbf{u}_h, \mathbf{v}_h)_{V_h} = \sum_{E \in \mathcal{P}_h} (\mathbf{u}_h, \mathbf{v}_h)_{\Lambda_S(E)}; \quad (\mathbf{u}_h, \mathbf{v}_h)_{\Lambda_S(E)} = \tilde{\mathbf{v}}_h^t \Lambda_S \tilde{\mathbf{u}}_h.$$

For this scalar product to be valid Λ_S must be positive definite. We make the following assumptions on Λ_S : there exist two positive constants \underline{c} and \bar{c} independent of h_E and E such that $\forall \mathbf{v}_h \in V_h$ and $\forall E \in \mathcal{P}_h$

$$(21) \quad \underline{c} h_E^{2-d} \sum_{F_i \in \partial E} \sum_{k \in \mathcal{N}_i^E} \tilde{v}_{ik}^2 \leq (\mathbf{v}_h, \mathbf{v}_h)_{\Lambda_S(E)} \leq \bar{c} h_E^{2-d} \sum_{F_i \in \partial E} \sum_{k \in \mathcal{N}_i^E} \tilde{v}_{ik}^2.$$

The validation and implication of this assumption is discussed in the last section. We also assume that

$$(22) \quad c_{\Lambda(E)} = \max_k \left(\frac{\|(\Lambda_A)\|_{L^\infty(E_k)}}{\min(\lambda_k)} \right),$$

is finite, where λ_k denotes the eigenvalues of $(\Lambda_S)_k$. This constant is used in an inequality similar to the Cauchy-Schwartz inequality. When the quadrature is symmetric the constant is zero and the standard Cauchy-Schwartz inequality is used.

We can now define the following norms based on the scalar products:

$$(23) \quad \|\mathbf{v}_h\|_{V_h}^2 = (\mathbf{v}_h, \mathbf{v}_h)_{V_h}, \quad \|\mathbf{v}_h\|_{V_h(E)}^2 = (\mathbf{v}_h, \mathbf{v}_h)_{\Lambda_S(E)} \quad \forall \mathbf{v}_h \in V_h$$

$$(24) \quad \|q_h\|_{X_h}^2 = (q_h, q_h)_{X_h}, \quad \|q_h\|_{X_h(E)}^2 = (q_h, q_h)_{0,E} \quad \forall q_h \in X_h.$$

3. Theoretical results

3.1. Well-posedness of the problem. To show the well-posedness of the problem, we will use the mesh dependent norms

$$(25) \quad \|\mathbf{v}_h\|_{\text{divh}}^2 = \sum_{E \in \mathcal{P}_h} \|\mathbf{v}_h\|_{\text{divh},E}^2 \quad \|\mathbf{v}_h\|_{\text{divh},E}^2 = \|\mathbf{v}_h\|_{V_h(E)}^2 + h_E^2 \|\nabla_h \cdot \mathbf{v}_h\|_{0,E}^2$$

$$(26) \quad \|\mathbf{v}\|_{1,h}^2 = \sum_{E \in \mathcal{P}_h} \|\mathbf{v}\|_{1,h,E}^2 \quad \|\mathbf{v}\|_{1,h,E}^2 = \|\mathbf{v}\|_{0,E}^2 + h_E^2 |\mathbf{v}|_{1,E}^2$$

in addition to the norms defined by means of the scalar products, (23) and (24).

The saddle-point problem (17) is well defined when the bilinear form $a(\mathbf{v}_h, \mathbf{w}_h) = \sum_{E \in \mathcal{P}_h} [\mathbf{v}_h, \mathbf{w}_h]_E$ is continuous and also coercive on the divergence-free subspace, while the inf-sup condition

$$(27) \quad \beta \|q_h\|_{X_h} \leq \sup_{\mathbf{v}_h \in V_h} \frac{(\nabla_h \cdot \mathbf{v}_h, q_h)_{X_h}}{\|\mathbf{v}_h\|_{\text{divh}}} \quad \forall q_h \in X_h,$$

must be satisfied with $\beta > 0$ and β independent of the number of elements in the grid.

The assumption (22) ensures the continuity of the bilinear form, since $\forall E \in \mathcal{P}_h$

$$(28) \quad \begin{aligned} [\mathbf{u}_h, \mathbf{v}_h]_E &= (\mathbf{u}_h, \mathbf{v}_h)_{\Lambda_S(E)} + \tilde{\mathbf{v}}_h^t \Lambda_A \tilde{\mathbf{u}}_h \leq (\mathbf{u}_h, \mathbf{v}_h)_{\Lambda_S(E)} + c_{\Lambda(E)} (\mathbf{u}_h, \mathbf{v}_h)_{\Lambda_S(E)} \\ &\leq (1 + c_{\Lambda(E)}) \|\mathbf{u}_h\|_{V_h(E)} \|\mathbf{v}_h\|_{V_h(E)} \end{aligned}$$

with $c_{\Lambda(E)}$ finite and thus

$$a(\mathbf{v}_h, \mathbf{w}_h) = \sum_{E \in \mathcal{P}_h} [\mathbf{u}_h, \mathbf{v}_h]_E \leq (1 + \max_E c_{\Lambda(E)}) \|\mathbf{u}_h\|_{V_h} \|\mathbf{v}_h\|_{V_h}.$$

The coercivity at the subspace

$$(29) \quad Z_h = \{\mathbf{v}_h \in V_h : (\nabla_h \cdot \mathbf{v}_h, q_h)_{X_h} = 0, \quad \forall q_h \in X_h\}$$

is evident since for any $\mathbf{v}_h \in Z_h$

$$(30) \quad \|\mathbf{v}_h\|_{\text{divh}}^2 = \|\mathbf{v}_h\|_{V_h}^2 = a(\mathbf{v}_h, \mathbf{v}_h).$$

The inf-sup condition can be proved as in [9] by first showing that for any $q_h \in X_h$ there exists $\mathbf{v}_h \in V_h$ such that $\nabla_h \cdot \mathbf{v}_h = q_h$. We define ψ such that $\Delta \psi = q_h$ when homogeneous boundary conditions are supplied. Setting $\mathbf{v} \in H(\text{div}, \Omega) = \nabla \psi$, the stability of the solution ensures that

$$(31) \quad \|\mathbf{v}\|_{1,h} \lesssim (1+h)\|q_h\|_{X_h}.$$

Setting $\mathbf{v}_h = \mathbf{v}^{\mathcal{I}}$ using the interpolation operator defined in (8) gives the sought for solution since

$$\nabla_h \cdot \mathbf{v}_h|_E = \nabla_h \cdot \mathbf{v}^{\mathcal{I}}|_E = \frac{1}{|E|}(\nabla \cdot \mathbf{v}, 1)_{0,E} = \frac{1}{|E|}(q_h, 1)_{0,E} = q_h|_E$$

Then the inf-sup condition (27) that needs to be proved reads

$$\sup \frac{(\nabla_h \cdot \mathbf{v}_h, q_h)_{X_h}}{\|\mathbf{v}_h\|_{\text{divh}}} = \sup \frac{\|q_h\|_{X_h}^2}{\|\mathbf{v}_h\|_{\text{divh}}} \geq \beta \|q_h\|_{X_h} \quad \forall q_h \in X_h,$$

that is

$$(32) \quad \|q_h\|_{X_h} \geq \beta \|\mathbf{v}_h\|_{\text{divh}} \quad \forall q_h \in X_h.$$

In Lemma 3 we prove that

$$\|\mathbf{v}_h\|_{\text{divh}} \lesssim \|\mathbf{v}\|_{1,h}$$

which together with (31) gives

$$(33) \quad \|\mathbf{v}_h\|_{\text{divh}} \lesssim (1+h)\|q_h\|_{X_h}$$

and thus we have satisfied the inf-sup condition (32).

In the following Lemma needed to prove the inf-sup condition we will make use of the trace inequality valid on shape regular domains:

$$(34) \quad \|\mathbf{v}_E\|_{0,F_i}^2 \leq c_F(h_E^{-1}\|\mathbf{v}_E\|_{0,E}^2 + h_E|\mathbf{v}_E|_{1,E}^2)$$

and the following hypothesis on mesh conformity:

$$(35) \quad c_{f1}h_E^{d-1} \leq |F|.$$

Lemma 3. *There exists a positive constant β such that $\forall \mathbf{v} \in (H^1(E))^d$ we have*

$$(36) \quad \beta \|\mathbf{v}^{\mathcal{I}}\|_{\text{divh}} \leq \|\mathbf{v}\|_{1,h}$$

Proof. The assumption (21) applied to the interpolation of \mathbf{v} states that

$$(37) \quad (\mathbf{v}^{\mathcal{I}}, \mathbf{v}^{\mathcal{I}})_{\Lambda_S(E)} \leq \bar{c}h_E^{2-d} \sum_{F_i \in \partial E} \sum_{k \in \mathcal{N}_i^E} (\tilde{v}_{ik}^{\mathcal{I}})^2.$$

Using the interpolation property (9) gives

$$\begin{aligned} \sum_{k \in \mathcal{N}_i^E} (\tilde{v}_{ik}^{\mathcal{I}})^2 &= \sum_{k \in \mathcal{N}_i^E} (\mathbf{v} \cdot \mathbf{n}_{Ei}, 1)_{0,F_{ik}}^2 \leq \sum_{k \in \mathcal{N}_i^E} \|\mathbf{v}\|_{0,F_{ik}}^2 |F_{ik}| \\ &\leq \sum_{k \in \mathcal{N}_i^E} \|\mathbf{v}\|_{0,F_{ik}}^2 \sum_{k \in \mathcal{N}_i^E} |F_{ik}| \leq \|\mathbf{v}\|_{0,F_i}^2 |F_i| \\ &\leq h_E^{d-1} \|\mathbf{v}\|_{0,F_i}^2 \end{aligned}$$

Inserting this result into (37) and using the trace inequality (34) we obtain

$$\begin{aligned}
 (\mathbf{v}^{\mathcal{I}}, \mathbf{v}^{\mathcal{I}})_{\Lambda_S(E)} &\leq \bar{c} h_E \sum_{F_i \in \partial E} \|\mathbf{v}\|_{0,F_i}^2 \\
 &\leq \bar{c} h_E \sum_{F_i \in \partial E} c_F (h_E^{-1} \|\mathbf{v}\|_{0,E}^2 + h_E |\mathbf{v}|_{1,E}^2) \\
 &\leq \bar{c} \sum_{F_i \in \partial E} c_F (\|\mathbf{v}\|_{0,E}^2 + h_E^2 |\mathbf{v}|_{1,E}^2) \\
 (38) \qquad \qquad \qquad &\leq \tilde{\beta}_E \|\mathbf{v}\|_{1,h,E}^2
 \end{aligned}$$

with

$$\tilde{\beta}_E = \bar{c} \max_{F \in \partial E} c_F$$

Furthermore, since

$$(\nabla_h \cdot \mathbf{v}^{\mathcal{I}}, 1)_{0,E} = (\nabla \cdot \mathbf{v}, 1)_{0,E} = (\Pi_0(\nabla \cdot \mathbf{v}), 1)_{0,E}$$

we have

$$(39) \qquad \qquad \qquad \|\nabla_h \cdot \mathbf{v}^{\mathcal{I}}\|_{0,E}^2 = \|\Pi_0(\nabla \cdot \mathbf{v})\|_{0,E}^2 \leq \|\nabla \cdot \mathbf{v}\|_{0,E}^2 \leq d |\mathbf{v}|_{1,E}^2$$

where d indicates the dimension (2 or 3). Combining (38) and (39) we obtain

$$\|\mathbf{v}^{\mathcal{I}}\|_{\text{divh},E}^2 \leq (\tilde{\beta}_E + d) \|\mathbf{v}\|_{1,h,E}^2$$

and thus (36), with

$$\beta = (\max_E \tilde{\beta}_E + d)^{-\frac{1}{2}}$$

□

3.2. Convergence. In the construction, the MPFA O-method uses the pressure at the barycenter of the element and the barycenters of the faces to make a linear interpolation in each subelement. We indicate this interpolator by $\mathcal{I}_O(p)$, and will use the following approximation results:

$$(40) \qquad \qquad \qquad \sum_{k \in \mathcal{N}^E} \|p - \mathcal{I}_O(p)\|_{0,E_k} \lesssim h_E^2 \|p\|_{2,E}.$$

$$(41) \qquad \qquad \qquad \sum_{k \in \mathcal{N}^E} \|\nabla(p - \mathcal{I}_O(p))\|_{0,E_k} \lesssim h_E \|p\|_{2,E}.$$

From (41) and the definition of the mesh-dependent norms (25) and (26), we then obtain

$$\begin{aligned}
 \|\nabla(p - \mathcal{I}_O(p))\|_{1,h,E} &\leq (\|\nabla(p - \mathcal{I}_O(p))\|_{0,E}^2 + h_E^2 |\nabla(p - \mathcal{I}_O(p))|_{1,E}^2)^{\frac{1}{2}} \\
 (42) \qquad \qquad \qquad &\lesssim h_E \|p\|_{2,E}.
 \end{aligned}$$

These approximation properties are local, not global, and if the solution is less regular than $H^2(\Omega)$ we will use the following: if $p \in H^{1+\alpha}(\Omega)$, then

$$(43) \qquad \qquad \qquad \|\nabla(p - \mathcal{I}_O(p))\|_{1,h,\Omega} \lesssim h^\alpha \|p\|_{1+\alpha,\Omega}.$$

The MPFA quadrature $[\cdot, \cdot]_E$ can be seen as an approximation of the integral $(K^{-1} \cdot, \cdot)_{0,E}$, which, using the divergence theorem on the element E for $q \in H^1(\Omega)$

and $\mathbf{v} \in H(\operatorname{div}, \Omega)$ is equal to

$$\begin{aligned} (K^{-1}K\nabla q, \mathbf{v})_{0,E} &= -(q, \nabla \cdot \mathbf{v})_{0,E} + (q, \mathbf{v} \cdot \mathbf{n}^E)_{0,\partial E} \\ &= -(q, \nabla \cdot \mathbf{v})_{0,E} + \sum_{F_i \in \partial E} |F_i|^{-1} (q, \mathbf{v} \cdot \mathbf{n}_i^E |F_i|)_{0,F_i}. \end{aligned}$$

We have rewritten the boundary integral to more easily see the analogy with the discrete fluxes. A similar relation is needed in the convergence proof for the MPFA method, indicating that the MPFA quadrature is exact on linear fields.

Lemma 4. *Let q be a continuous function, and let $\mathcal{I}_O(q)$ be the interpolator as described. Then the MPFA method satisfies the following discrete divergence theorem:*

$$(44) \quad \sum_{k \in \mathcal{N}^E} [K_0^E \nabla \mathcal{I}_O(q), \mathbf{v}_h]_{E_k} = -q(\bar{\mathbf{x}}_0) |E| \nabla_h \cdot \mathbf{v}_h + \sum_{F_i \in \partial E} q(\bar{\mathbf{x}}_i) \tilde{v}_i^E \quad \forall \mathbf{v}_h \in V_h.$$

Proof. The partial fluxes of $K_0^E \nabla \mathcal{I}_O(q)$ on the external faces of E_k are equal to $Q_k^t K_0^E \nabla \mathcal{I}_O(q)$, as $K_0^E \nabla \mathcal{I}_O(q)$ is constant and each column of the matrix Q_k corresponds to the integral of the normal vector on F_{ik} . Using the quadrature of the MPFA method (see (13) and (14)), the left-hand side of (44) is

$$\begin{aligned} \sum_{k \in \mathcal{N}^E} [K_0^E \nabla \mathcal{I}_O(q), \mathbf{v}_h]_{E_k} &= \sum_k \tilde{\mathbf{v}}_k^t \Lambda_k Q_k^t K_0^E \nabla \mathcal{I}_O(q) \\ &= \sum_k \tilde{\mathbf{v}}_k^t R_k (K_0^E)^{-1} Q_k^{-t} Q_k^t K_0^E \nabla \mathcal{I}_O(q) \\ (45) \quad &= \sum_k \tilde{\mathbf{v}}_k^t R_k \nabla \mathcal{I}_O(q). \end{aligned}$$

The right hand side of (44) is equal to

$$(46) \quad \sum_{F_i \in \partial E} \left(\sum_{k \in \mathcal{N}_i^E} \tilde{v}_{ik}^E \right) (q(\bar{\mathbf{x}}_i) - q(\bar{\mathbf{x}}_0^E)) = \sum_k \tilde{\mathbf{v}}_k^t R_k \nabla \mathcal{I}_O(q)$$

which proves that (46) is equal to (45) for all $\tilde{\mathbf{v}}_k$, and thus (44) is satisfied for all $\mathbf{v}_h \in V_h$. \square

We note that since q is continuous, the second term on the right-hand side of (44) sums to zero over the elements, and we have

$$(47) \quad \sum_{E \in \mathcal{P}_h} [K_0^E \nabla \mathcal{I}_O(q), \mathbf{v}_h]_E = - \sum_{E \in \mathcal{P}_h} q(\bar{\mathbf{x}}_0) |E| \nabla_h \cdot \mathbf{v}_h.$$

By comparing with the MPFA formulation we see that the pressure p_h is an approximation of the pressure in the cell centers. The change of sign is due to the definition of the Darcy velocity (defined as opposed to the gradient of the pressure). We also note that if q is a linear function over the whole element, then

$$(q, \nabla_h \cdot \mathbf{v}_h)_{0,E} = (q, 1)_{0,E} \nabla_h \cdot \mathbf{v}_h = |E| q(\bar{\mathbf{x}}_0) \nabla_h \cdot \mathbf{v}_h$$

and

$$\sum_{F_i \in \partial E} |F_i|^{-1} (q, \tilde{v}_i^E)_{0,F_i} = \sum_{F_i \in \partial E} |F_i|^{-1} (q, 1)_{0,F_i} \tilde{v}_i^E = \sum_{F_i \in \partial E} q(\bar{\mathbf{x}}_i) \tilde{v}_i^E.$$

This brings the comparison with the divergence theorem closer, as we have

$$\sum_{k \in \mathcal{N}^E} [K_0^E \nabla \mathcal{I}_O(q), \mathbf{v}_h]_{E_k} = -(q, \nabla_h \cdot \mathbf{v}_h)_{0,E} + \sum_{F_i \in \partial E} |F_i|^{-1} (q, \tilde{v}_i^E)_{0,F_i}$$

Theorem 5. Let (p, \mathbf{u}) be the solution of the continuous problem (2), and let (p_h, \mathbf{u}_h) be the solution of the discrete problem (17). Let $\mathbf{u}^I \in V_h$ be the interpolant of \mathbf{u} defined by (8). Then, if $p \in H^{1+\alpha}(\Omega)$ with $0 \leq \alpha \leq 1$,

$$(48) \quad \|\mathbf{u}^I - \mathbf{u}_h\|_{V_h} \lesssim h^\alpha \|p\|_{1+\alpha, \Omega}.$$

Proof. We note that $\forall \mathbf{u}_h \in V_h$,

$$\|\mathbf{u}_h\|_{V_h}^2 = \sum_{E \in \mathcal{P}_h} (\mathbf{u}_h, \mathbf{u}_h)_{\Lambda_S(E)} = \sum_{E \in \mathcal{P}_h} [\mathbf{u}_h, \mathbf{u}_h]_E.$$

Then, using the discrete problem (17),

$$\begin{aligned} \|\mathbf{u}^I - \mathbf{u}_h\|_{V_h}^2 &= \sum_{E \in \mathcal{P}_h} [\mathbf{u}^I - \mathbf{u}_h, \mathbf{u}^I - \mathbf{u}_h]_E \\ &= \sum_{E \in \mathcal{P}_h} [\mathbf{u}^I, \mathbf{u}^I - \mathbf{u}_h]_E - \sum_{E \in \mathcal{P}_h} [\mathbf{u}_h, \mathbf{u}^I - \mathbf{u}_h]_E \\ &= \sum_{E \in \mathcal{P}_h} [\mathbf{u}^I, \mathbf{u}^I - \mathbf{u}_h]_E - (p_h, \nabla_h \cdot (\mathbf{u}^I - \mathbf{u}_h))_{X_h} \end{aligned}$$

where the second term on the right-hand side is zero due to (11) and (17). Adding and subtracting equal terms we obtain

$$\begin{aligned} \|\mathbf{u}^I - \mathbf{u}_h\|_{V_h}^2 &= \sum_{E \in \mathcal{P}_h} [\mathbf{u}^I, \mathbf{u}^I - \mathbf{u}_h]_E \\ &= \sum_{E \in \mathcal{P}_h} [(-K\nabla p)^I + (K\nabla \mathcal{I}_O(p))^I, \mathbf{u}^I - \mathbf{u}_h]_E \\ &\quad + \sum_{E \in \mathcal{P}_h} [(-K\nabla \mathcal{I}_O(p))^I + (K_0^E \nabla \mathcal{I}_O(p))^I, \mathbf{u}^I - \mathbf{u}_h]_E \\ &\quad + \sum_{E \in \mathcal{P}_h} [(-K_0^E \nabla \mathcal{I}_O(p))^I, \mathbf{u}^I - \mathbf{u}_h]_E \\ (49) \quad &= I_1 + I_2 + I_3 \end{aligned}$$

For the first term we use (28) to obtain

$$\begin{aligned} |I_1| &= \left| \sum_{E \in \mathcal{P}_h} [(-K\nabla p)^I + (K\nabla \mathcal{I}_O(p))^I, \mathbf{u}^I - \mathbf{u}_h]_E \right| \\ &\leq \sum_{E \in \mathcal{P}_h} (1 + c_{\Lambda(E)}) \|(K\nabla(p - \mathcal{I}_O(p)))^I\|_{V_h(E)} \|\mathbf{u}^I - \mathbf{u}_h\|_{V_h(E)}. \end{aligned}$$

From (38) we have

$$\|(K\nabla(p - \mathcal{I}_O(p)))^I\|_{V_h(E)} \leq \tilde{\beta}_E^{\frac{1}{2}} \|K\nabla(p - \mathcal{I}_O(p))\|_{1,h,E}$$

Using the approximation result (42) or (43) we then obtain

$$\sum_{E \in \mathcal{P}_h} \tilde{\beta}_E^{\frac{1}{2}} \|K\nabla(p - \mathcal{I}_O(p))\|_{1,h,E} \lesssim \max_E (\|K\|_{L^\infty(E)}) h^\alpha \|p\|_{1+\alpha, E}$$

and thus

$$(50) \quad |I_1| \lesssim h^\alpha \|p\|_{1+\alpha, \Omega} \|\mathbf{u}^I - \mathbf{u}_h\|_{V_h}.$$

For the second term we first use (28) and the assumption on the permeability tensor (12) to obtain

$$\begin{aligned}
 |I_2| &= \left| \sum_{E \in \mathcal{P}_h} [(-K + K_0^E) \nabla \mathcal{I}_O(p)]^T, \mathbf{u}^T - \mathbf{u}_h \right|_E \\
 &\leq \sum_{E \in \mathcal{P}_h} \|K - K_0^E\|_{L^\infty(E)} (1 + c_{\Lambda(E)}) \|(\nabla \mathcal{I}_O(p))^T\|_{V_h(E)} \|\mathbf{u}^T - \mathbf{u}_h\|_{V_h(E)} \\
 &\lesssim \sum_{E \in \mathcal{P}_h} h_E \|(\nabla \mathcal{I}_O(p))^T\|_{V_h(E)} \|\mathbf{u}^T - \mathbf{u}_h\|_{V_h(E)}.
 \end{aligned}$$

From (38) and adding and subtracting the function p we have

$$\begin{aligned}
 \|(\nabla \mathcal{I}_O(p))^T\|_{V_h(E)} &\leq \tilde{\beta}_E^{\frac{1}{2}} \|\nabla \mathcal{I}_O(p)\|_{1,h,E} \\
 &\leq \tilde{\beta}_E^{\frac{1}{2}} (\|\nabla p\|_{1,h,E} + \|\nabla(p - \mathcal{I}_O(p))\|_{1,h,E}) \\
 (51) \qquad \qquad \qquad &\lesssim \|\nabla p\|_{0,E}
 \end{aligned}$$

The second term of (49) is therefore controlled by

$$(52) \qquad |I_2| \lesssim \sum_{E \in \mathcal{P}_h} h_E \|p\|_{1,E} \|\mathbf{u}^T - \mathbf{u}_h\|_{V_h(E)}.$$

For the third term we note that $(K_0^E \nabla \mathcal{I}_O(p))^T = K_0^E \nabla \mathcal{I}_O(p)$ and apply Lemma 4 to obtain

$$\begin{aligned}
 I_3 &= \sum_{E \in \mathcal{P}_h} [(-K_0^E \nabla \mathcal{I}_O(p))^T, \mathbf{u}^T - \mathbf{u}_h]_E \\
 &= - \sum_{E \in \mathcal{P}_h} [K_0^E \nabla \mathcal{I}_O(p), \mathbf{u}^T - \mathbf{u}_h]_E \\
 &= \sum_{E \in \mathcal{P}_h} p(\bar{\mathbf{x}}_0) \sum_{F_i \in \partial E} \sum_{k \in \mathcal{N}_i^E} (\tilde{u}_{ik}^T - \tilde{u}_{h,ik})
 \end{aligned}$$

where \tilde{u}_{ik}^T and $\tilde{u}_{h,ik}$ indicate the partial side fluxes of respectively the interpolated exact solution and the approximated solution. We have here used the fact that the interpolator is continuous at the barycenters of the faces and takes the value zero at the boundary. For the fluxes we have that

$$\sum_{k \in \mathcal{N}_i^E} |\tilde{u}_{ik}^T - \tilde{u}_{h,ik}| \leq m_i^{\frac{1}{2}} \left(\sum_{k \in \mathcal{N}_i^E} |\tilde{u}_{ik}^T - \tilde{u}_{h,ik}|^2 \right)^{\frac{1}{2}}.$$

Applying the assumption (21) we obtain

$$\begin{aligned}
 |I_3| &\lesssim \sum_E |p(\bar{\mathbf{x}}_0)| h_E^{d/2-1} \|\mathbf{u}^T - \mathbf{u}_h\|_{V_h(E)} \\
 &\lesssim h^{d-1} \|p\|_{0,\Omega} \|\mathbf{u}^T - \mathbf{u}_h\|_{V_h}.
 \end{aligned}$$

Summing I_1 , I_2 and I_3 and simplifying we obtain Theorem 5. □

In the following theorem the proof is based on the well-posedness of the dual problem

$$(53) \qquad \begin{cases} -\nabla \cdot (K \nabla \psi) = \Pi_0 p - p_h & \text{in } \Omega \\ \psi = 0 & \text{on } \partial\Omega. \end{cases}$$

where $\Pi_0 p$ indicates the L^2 projection of p on each element E . When K is continuous and the domain is convex we have the stability result

$$(54) \quad \|\psi\|_{2,\Omega} \lesssim \lambda_K^{-\frac{1}{2}} \|\Pi_0 p - p_h\|_{X_h}$$

where λ_K indicates the largest eigenvalue of K . In general when K is discontinuous the hypothesis of a convex domain is not sufficient to assure (54), but will require assumptions on the distribution of K .

Theorem 6. *Let (p, \mathbf{u}) be the solution of the continuous problem (2), and let (p_h, \mathbf{u}_h) be the solution of the discrete problem (17). Let $\Pi_0 p$ indicate the L^2 projection of p on each element E . Assume (54) to be valid. Then, if $p \in H^{1+\alpha}(\Omega)$ with $0 \leq \alpha \leq 1$,*

$$\|p_h - \Pi_0 p\|_{X_h} \lesssim h^\alpha \|p\|_{1+\alpha,\Omega}.$$

Proof. We use the dual problem (53) in its weak form and the MPFA formulation (17) to obtain

$$(55) \quad \begin{aligned} \|p_h - \Pi_0 p\|_{X_h}^2 &= (p_h - \Pi_0 p, \nabla \cdot (K \nabla \psi))_{X_h} \\ &= -[\mathbf{u}^T - \mathbf{u}_h, (K \nabla \psi)^T]_{V_h} + [\mathbf{u}^T, (K \nabla \psi)^T]_{V_h} - (\Pi_0 p, \nabla \cdot (K \nabla \psi))_{0,\Omega} \\ &= \text{IV} + \text{V} + \text{VI}. \end{aligned}$$

For the first term we use the result from the previous theorem (48):

$$|\text{IV}| \lesssim \|\mathbf{u}^T - \mathbf{u}_h\|_{V_h} \|(K \nabla \psi)^T\|_{V_h} \lesssim h^\alpha \|p\|_{1+\alpha,\Omega} \|\psi\|_{2,\Omega}.$$

The second term we expand into three parts as in the proof of the previous theorem:

$$\begin{aligned} \text{V} &= \sum_{E \in \mathcal{P}_h} [(-K \nabla p)^T + (K \nabla \mathcal{I}_O(p))^T, (K \nabla \psi)^T]_E \\ &\quad + \sum_{E \in \mathcal{P}_h} [(-K \nabla \mathcal{I}_O(p))^T + (K_0^E \nabla \mathcal{I}_O(p))^T, (K \nabla \psi)^T]_E \\ &\quad + \sum_{E \in \mathcal{P}_h} [(-K_0^E \nabla \mathcal{I}_O(p))^T, (K \nabla \psi)^T]_E \\ &= \text{Va} + \text{Vb} + \text{Vc}. \end{aligned}$$

As previously we can show that

$$|\text{Va}| + |\text{Vb}| \lesssim h^\alpha \|p\|_{1+\alpha,\Omega} \|\psi\|_{2,\Omega}.$$

Examining the remaining terms and using Lemma 4 in the form (47), we have

$$(56) \quad \begin{aligned} |\text{Vc} + \text{VI}| &= \left| \sum_{E \in \mathcal{P}_h} p(\bar{x}_0^E) (1, p_h - \Pi_0 p)_{0,E} - (\Pi_0 p, p_h - \Pi_0 p)_{0,\Omega} \right| \\ &\leq \|p(\bar{x}_0^E) - \Pi_0 p\|_{X_h} \|p_h - \Pi_0 p\|_{X_h} \\ &\lesssim h \|p\|_{1,\Omega} \|p_h - \Pi_0 p\|_{X_h}. \end{aligned}$$

Inserting the results in (55) and using the stability result (54), we can simplify the term $\|p_h - \Pi_0 p\|_{X_h}$ to obtain the final result. \square

4. Numerical examples

This section contains some numerical examples and a discussion of the convergence behavior with particular emphasis on the limitation of the analysis. A fundamental part of the convergence analysis in the previous section is the assumption regarding the symmetric matrix Λ_S , namely (21), required to establish coercivity and convergence of the method. This condition is linked to the definition of the MPFA dual mesh and the permeability tensor K . To fulfill the lower bound of (21), the eigenvalues of $(\Lambda_S)_k$, cf. eq (14), for all k of E and all $E \in \mathcal{P}_h$ have to be strictly positive. Positive eigenvalues means that the determinant of the matrix is positive. For a 2×2 symmetric matrix with positive diagonal elements the inverse is also true, and makes an easy test for positive definiteness.

4.1. Polyhedral 2D mesh. In 2D it can easily be shown by dividing Λ^E into a symmetric and a skew-symmetric part, cf. (20), that the determinants (indicated by \det) fulfill the following relation:

$$\det \Lambda^E = \det(\Lambda_S) + \det(\Lambda_A).$$

Furthermore we note that

$$\det \Lambda_k = \det R_k \det(K_0^E)^{-1} \det Q_k^{-t} = \frac{\det R_k}{\det Q_k} \det(K_0^E)^{-1}.$$

The determinant of R_k can be visualised as the area spanned by the two vectors $\bar{\mathbf{x}}_{i1}^E - \bar{\mathbf{x}}_0^E$ and $\bar{\mathbf{x}}_{i2}^E - \bar{\mathbf{x}}_0^E$. Similarly, $\det Q_k$ is the area spanned by $\tilde{\mathbf{n}}_{i1}$ and $\tilde{\mathbf{n}}_{i2}$. We denote the respective areas A_R and A_Q . On sub-cell k we then have

$$\begin{aligned} \det((\Lambda_s)_k) &= \frac{1}{\det K_0^E} \frac{A_R}{A_Q} \\ &\quad - \frac{1}{4A_Q^2} [(\bar{\mathbf{x}}_{i1}^E - \bar{\mathbf{x}}_0^E)^t (K_0^E)^{-1} (\mathbf{x}_k^E - \bar{\mathbf{x}}_{i1}^E) - (\bar{\mathbf{x}}_{i2}^E - \bar{\mathbf{x}}_0^E)^t (K_0^E)^{-1} (\mathbf{x}_k^E - \bar{\mathbf{x}}_{i2}^E)]^2 \end{aligned}$$

where \mathbf{x}_k indicates the coordinate of the node k , and $\mathbf{x}_k - \bar{\mathbf{x}}_{ij}$ is a vector perpendicular to $\tilde{\mathbf{n}}_{ij}$. For K -orthogonal meshes the last term vanishes, the method is symmetric and the lower bound is always fulfilled. For other quadrilateral and general polyhedral meshes the criteria in equation (21) will be the dominant mesh restriction. For triangulations this restriction can be avoided, since there exists a symmetric MPFA with satisfactory qualities, as shown by Klausen et al. in [18].

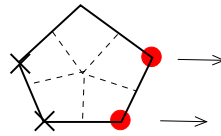


FIGURE 4. The cell is fixed in vertices marked with a cross, while the vertices marked with full circles are pulled out until the criteria (21) is violated.

In our first test we look at a uniform pentagram with edge length equal to h . The pentagram is deformed by pulling two vertices uniformly out to the right, as indicated in Figure 4. The two vertices marked with a cross are fixed, while the last vertex is kept at the the axis of symmetry. For $K = I$ the criteria (21) breaks down for at least one subelement when we have pulled the vertices out by $2.6h$. Here h denotes the original edge length. This indicates that the allowed deformation is unfortunately quite small.

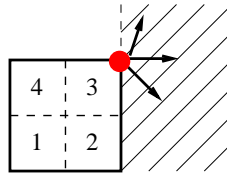


FIGURE 5. The vertex marked with a full circle is pulled out in all directions of the adjacent plane.

For our next test regarding the limitation of criteria (21) we look at a unit square with the upper right vertex placed at the origin of the plane. This vertex is then displaced in the directions contained in a half plane, as indicated in Figure 5. We set the permeability $K = I$, and number the subelements from 1 through 4 as shown. For each subelement we investigate the deformation needed for one of the eigenvalues of $(\Lambda_S)_k$ to approach zero. The result is presented in Figure 6. Each line indicates the deformation allowed in the horizontal and vertical directions before the criteria (21) breaks down. To the left of the line the criteria holds. Note that for subelement 3, the criteria (21) is satisfied for the displacements shown.

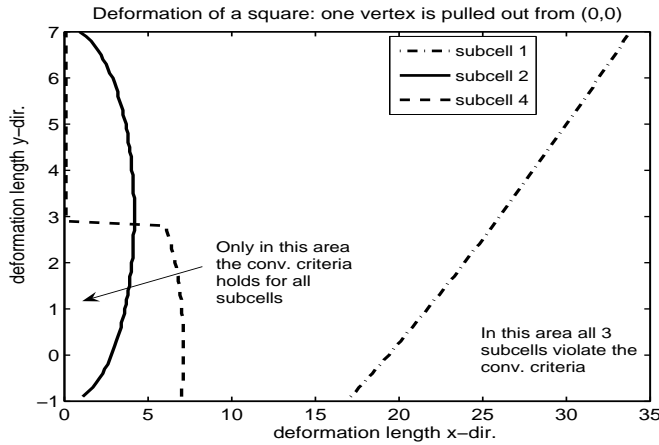


FIGURE 6. Limitations of the criteria (21) regarding the deformation of a square when the upper right vertex, originally placed in the origin of a plane, is displaced in directions as illustrated in Figure 5.

Finally we repeat the previous test, but now we use an anisotropic permeability tensor whose principal axes are aligned with the x - and the y -direction, namely $K = \text{diag}(\beta, 1)$ with $\beta \in \{1, 10, 100, 500\}$. For each value of β the line in the half-plane for which the criteria (21) breaks down for at least one sub-cell is drawn. The result is shown in Figure 7, where the area containing the origin indicates the deformations permitted. We see that as the diffusion in the x -direction is increased (increasing β), the deformation permitted in the same direction is increased as well, while the deformation in the y -direction becomes more limited. This indicates the reason why the MPFA method is more sensitive regarding strong anisotropies compared with the mimetic finite difference method.

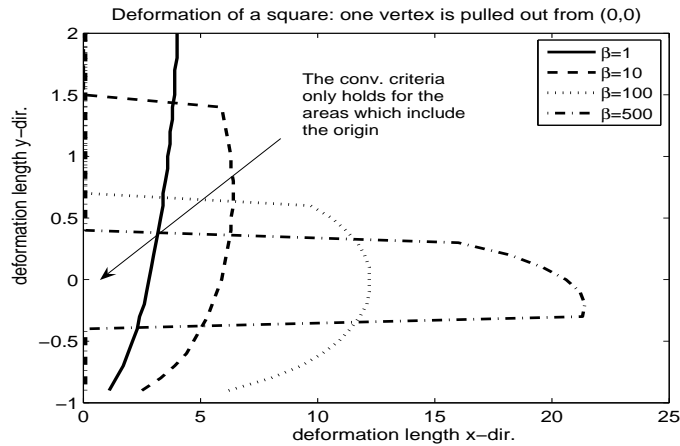


FIGURE 7. *Limitation of the criteria (21) regarding the deformation of a square when different values of $K = \text{diag}(\beta, 1)$ are considered.*

4.2. Deformed cube mesh. We have tested different deformations of cubes, starting from a uniform h -sized cube and pulling out one, two, or more vertices. We note limitations similar to the 2D situation, and the criteria mainly holds until we have stretched the edges by a factor between 2 and 4 with $K = I$. One specific example is the saddle-roof box, shown in Figure 8. Starting with the uniform box of size $h \times h \times h$ we deform the upper face. Two vertices situated opposite each other on the same face are pulled upwards creating a bilinear saddle surface on top of the box. The criteria (21) breaks down for at least one of the sub-cells when the original h -sized edge are stretched to $3.45h$. Another example is the truncated pyramid, where the upper square is of size $h \times h$ while the bottom is stretch out to an $\alpha h \times \alpha h$ - square, cf. Figure 8. In this case the criteria (21) breaks down for at least one of the sub-cells when α reach 2.75.

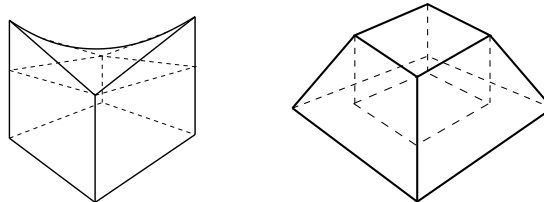


FIGURE 8. *The cells are stretched from a uniform box, to a saddle roof box and a truncated pyramid, until the criteria (21) is no longer fulfilled.*

4.3. Convergence examples. Since Λ_k^E depends on both the cell shape and K (see (14)), the criteria (21) is put to the test both by deforming the mesh and by varying the permeability. In Table 1 and 2 we show a numerical example in 2D with $K = \text{diag}(\beta, 1)$ where β is increased from 1 to 1000. The mesh is shown in Figure 9, where refinement is a replication of the shown 4×4 mesh. The subelements are marked with dashed lines. From Remark 1 we know that the subelements in 2D always become quadrilateral, and on that background we have chosen a

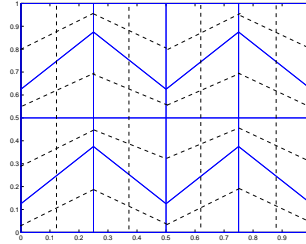


FIGURE 9. The 4×4 mesh, used for the numerical test shown in Table 1 and 2. The quadrilateral subelements are marked with dashed lines.

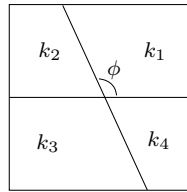


FIGURE 10. Subdomains 1-4.

quadrilateral mesh for these numerical tests. The mesh is chosen such that the quadrilateral shape of the subelements remains the same when the mesh is refined, while the anisotropy is increased. This way we control the increased roughness of Λ_k^E which goes into the criteria (21). The data is chosen so that $p(x, y) = \cos(2\pi x) \cos(2\pi y)$ is the exact solution on the domain which is the unit square. In order to test the behavior of the flux calculated by the MPFA O-method when Λ_S has negative eigenvalues we must modify the norm we have used, as it is no longer valid as a norm. In Table 2 the convergence of the flux is measured in the following norm:

$$\|\mathbf{v}_h\|_{V_h^*}^2 = \sum_{E \in \mathcal{P}_h} (\mathbf{v}_h, \mathbf{v}_h)_{V_h^*(E)}, \quad (\mathbf{v}_h, \mathbf{v}_h)_{V_h^*(E)} = \beta^{-1} (\mathbf{v}_h, \mathbf{v}_h)_{0,E} \quad \forall \mathbf{v}_h \in V_h.$$

For the error in the pressure we use the X_h -norm as previously defined. The convergence results and the percentage of sub-cells for which criteria (21) breaks down are found in Table 1 for the pressure and Table 2 for the flux. In the chosen norms the flux converges with optimal first order, while the pressure converges with second order. It seems then that the criteria (21) is not sharp in the sense that convergence can be obtained in comparable norms when the criteria is not fulfilled.

To illustrate the behavior of MPFA around a singularity, where $p \in H^{1+\xi-\epsilon}$, $0 < \xi < 1$, for all $\epsilon > 0$, we assume the permeability to be isotropic in each of the four subdomains of Figure 10. The permeability is given by a scalar k_i for $i = 1, \dots, 4$. Changing to polar coordinates (r, θ) gives the solution in each of the subdomains, with appropriate boundary conditions

$$(57) \quad p(r, \theta) = r^\xi (a_i \cos(\xi\theta) + b_i \sin(\xi\theta))$$

for $i = 1, 2, 3, 4$. The coefficients a_i, b_i for $i = 1, \dots, 4$ and ξ are found from the permeabilities and the shape of the subdomains such that equation (57) is a solution of (1) on the entire domain. The results are shown in Table 3, where the convergence rate of the pressure and velocity at a refinement step from 64 to 128

β	1	10	20	50	100	1000
8×8	$2.42e-2$	$7.66e-2$	$1.08e-1$	$1.56e-1$	$1.91e-1$	$2.45e-1$
16×16	$5.90e-3$	$1.78e-2$	$2.55e-2$	$3.99e-2$	$5.49e-2$	$1.04e-1$
32×32	$1.50e-3$	$4.00e-3$	$5.50e-3$	$8.70e-3$	$1.25e-2$	$3.75e-2$
64×64	$4.00e-4$	$9.00e-4$	$1.20e-3$	$1.80e-3$	$2.50e-3$	$9.80e-3$
Conv. rate last step	1.98	2.01	2.19	2.31	2.31	1.93
% E_k violating (21)	0	25	50	75	100	100

TABLE 1. The error $\|p_h - p(x_{\text{cell center}})\|_{X_h}$ and the percentage of subelements violating (21).

β	1	10	20	50	100	1000
8×8	1.04	1.35	1.49	1.65	1.75	1.89
16×16	0.50	0.61	0.66	0.73	0.78	0.91
32×32	0.25	0.29	0.31	0.33	0.35	0.42
64×64	0.12	0.14	0.15	0.15	0.16	0.19
Conv. rate last step	1.01	1.02	1.04	1.08	1.12	1.17
% E_K violating (21)	0	25	50	75	100	100

TABLE 2. The error $\|\mathbf{u}_h - (\mathbf{u}(x_{\text{edge center}}))^T\|_{V_{h^*}}$ and the percentage of subelements violating (21).

$k_{1,3}/k_{2,4}$	1/2	1/5	1/15	1/40	1/100
ξ	0.78	0.54	0.32	0.20	0.12
$O(\ p_h - p(x_{\text{cell center}})\ _{X_h})$	1.56	1.07	0.62	0.34	0.19
$O(\ \mathbf{u}_h - (\mathbf{u}(x_{\text{edge center}}))^T\ _{V_{h^*}})$	0.81	0.56	0.33	0.15	0.04
% E_k violating (21)	0	0	0	0	0

TABLE 3. The order of convergence of the pressure and velocity error around a singularity.

square cell in each direction and with $\phi = \pi/2$. In [13] a wide range of similar examples are tested and discussed for MPFA on challenging quadrilateral grids and different ϕ values, all showing the same trends as shown in Table 3. The order of convergence around a singular corner is $O(\xi)$ for the velocities and $O(2\xi)$ for the pressure. Around strong singularities there seems to be a need for further refinement of the mesh to reach asymptotic convergence.

Acknowledgments

This research was supported by VISTA, c/o the Norwegian Academy of Science and Letters.

References

- [1] J. Aarnes, S. Krogstad, K.-A. Lie, "Multiscale mixed/mimetic methods on corner-point grids." *Comput. Geosci.* 12 (2008), no. 3, pp. 297–315.
- [2] I. Aavatsmark, T. Barkve, Ø. Bøe, and T. Mannseth "Discretization on unstructured grids for inhomogeneous, anisotropic media. I. Derivation of the methods, II. Discussion and numerical results.," *SIAM J. Sci. Comput.*, 19 (1998), pp. 1700–1736.

- [3] I. Aavatsmark, “An introduction to multipoint flux approximations for quadrilateral grids”, *Comput. Geosci.*, 6 (2002), pp. 404–432.
- [4] I. Aavatsmark, “Interpretation of a two-point flux stencil for skew parallelogram grids”, *Comput. Geosci.*, 11 (2007), pp. 199–206.
- [5] I. Aavatsmark, G.T. Eigestad, R.A. Klausen, M.F. Wheeler, I. Yotov. “Convergence of a symmetric MPFA method on quadrilateral grids”, *Comput. Geosci.* 11 (2007), no. 4, pp. 333–345.
- [6] I. Aavatsmark, G. T. Eigestad, B. T. Mallison and J. M. Nordbotten “A compact multipoint flux approximation method with improved robustness” *Numer. Methods Partial Diff. Eqns.*, 24 (2008), pp. 1329–1360.
- [7] L. Agelas and R. Masson “Convergence of finite volume MPFA O type schemes for heterogeneous anisotropic diffusion problems on general meshes” *C. R. Acad. Sci. Paris*, 246 (2008), pp. 1007–1012.
- [8] M. Bause, J. Hoffmann, and P. Knabner, “First-order convergence of multi-point flux approximation on triangular grids and comparison with mixed finite element methods.” *Numer. Math.* 116 (2010), no. 1, pp. 1–29.
- [9] F. Brezzi, K. Lipnikov and M. Shashkov, “Convergence of mimetic finite difference method for diffusion problems on polyhedral meshes”, *SIAM J. Numer. Anal.* 5 (2005), pp. 1872–1896.
- [10] F. Brezzi, K. Lipnikov and M. Shashkov, “Convergence of mimetic finite difference method for diffusion problems on polyhedral meshes with curved faces”, *Math. Models Methods Appl. Sci.* 2 (2006), pp. 275–297.
- [11] M. G. Edwards and C. F. Rogers, “Finite volume discretization with imposed flux continuity for the general tensor pressure equation”, *Comput. Geosci.*, 2 (1998), pp. 259–290.
- [12] M. G. Edwards, “Unstructured, control-volume distributed, full-tensor finite-volume schemes with flow based grids”, *Comput. Geosci.*, 6 (2002), pp. 433–452.
- [13] G. T. Eigestad and R. A. Klausen, “On the convergence of the multi-point flux approximation O-method: Numerical experiments for discontinuous permeability”, *Numer. Methods Partial Diff. Eqns.*, 21 (2005), pp. 1079–1098.
- [14] R. Eymard, T. Gallouet and R. Herbin, “The finite volume method”, Ph. Charlet and J.L. Lions eds, North Holland 2000.
- [15] R. Eymard, T. Gallouet and R. Herbin, “Discretization schemes for heterogeneous and anisotropic diffusion problems on general nonconforming meshes SUSHI: a scheme using stabilization and hybrid interfaces”, *IMA J Numer. Anal.*, 30 (2009) no.4, pp. 1009–1043.
- [16] R. Ingram, M. Wheeler, and I. Yotov, “A multipoint flux mixed finite element method on hexahedra.” *SIAM J. Numer. Anal.* 48 (2010), no. 4, pp. 1281–1312.
- [17] R.A. Klausen, and A.F. Stephansen “On Rough Grids Convergence and Reproduction of Uniform Flow.”, 12th European Conference on the Mathematics of Oil Recovery Oxford, UK, September 06 - 09, 2010.
- [18] R. A. Klausen, F.A. Radu and G.T. Eigestad, “Convergence of MPFA on triangulations and for Richards’ equation”, *Internat. J. Numer. Methods Fluids* 58 (2008), no. 12, 1327–1351.
- [19] R. A. Klausen and T. F. Russell, “Relationships among some locally conservative discretization methods which handle discontinuous coefficients”, *Comput. Geosci.* 8 (2004), no. 4, pp. 341–377.
- [20] R. A. Klausen and A. F. Stephansen, “Mimetic MPFA.”, *Proc.11th European Conference on the Mathematics of Oil Recovery*, 2008.
- [21] R. A. Klausen and R. Winther, “Convergence of multi point flux approximations on quadrilateral grids”, *Numer. Methods for PDE’s*, 22 (2006), pp. 1438–1454.
- [22] R. A. Klausen and R. Winther, “Robust convergence of multi point flux approximation on rough grids”, *Numer. Math.* 104 (2006), pp. 317–337.
- [23] K. Lipnikov, M. Shashkov and I. Yotov, “Local flux mimetic finite difference methods”, *Numer. Math.* 1 (2009), pp. 115–152.
- [24] M. Pal, M. G. Edwards and A. R. Lamb, “Convergence study of a family of flux-continuous, finite-volume schemes for the general tensor pressure equation”, *Internat. J. Numer. Methods Fluids* 51 (2006), pp. 1177–1203.
- [25] M. Pal and M. Edwards, “q-families of CVD(MPFA) schemes on general elements: numerical convergence and the maximum principle”, *Arch. Comput. Methods Eng.* 17 (2010), no. 2, pp. 137–189.
- [26] M. Petzoldt, “Regularity and error estimators for elliptic problems with discontinuous coefficients”, Ph.D. thesis, FU Berlin (2001), <http://www.diss.fu-berlin.de/diss>

- [27] G. Strang and G. J. Fix, “An Analysis of the Finite Element Method”. Wiley, New York, 1973.
- [28] M. Vohralik, “Equivalence between mixed finite element and multi-point finite volume methods”, C. R. Acad. Sci. Paris., Ser. I 339 (2004).
- [29] M. F. Wheeler and I. Yotov, “A multipoint flux mixed finite element method”, SIAM J. Numer. Anal. 44 (2006), pp. 2082–2106.
- [30] S. F. Matringe, R. Juanes and H. A. Tchelepi, “Convergence of MPFA on hexahedra”, Proc. SPE Reservoir Simulation Symposium, 2009.
- [31] D. K. Ponting, “Corner point geometry in reservoir simulation”, Proc. of the 1st European Conference on Mathematics of Oil Recovery, Cambridge, Clarendon Press (1989) pp. 4565.

Centre of Mathematics for Applications, University of Oslo, Norway
E-mail: `r.a.klausen@cma.uio.no`

Uni CIPR, Uni Research, Norway
E-mail: `annette.stephansen@uni.no`